RSC Advances

ROYAL SOCIETY OF CHEMISTRY

PAPER

View Article Online
View Journal | View Issue

Check for updates

Cite this: *RSC Adv.*, 2025, **15**, 8878

A zinc oxide–silver nanocomposite-based SERS nanoplatform for ultrasensitive ofloxacin determination in beef and an ophthalmic solution: effects of ZnO and ZnO content on electron transfer and SERS enhancements†

Dao Thi Nguyet Nga, ‡[a] Ha Anh Nguyen, ‡*[a] Nguyen Thi Hoa,[a] Nguyen Ngoc Huyen, [a] Ngo Xuan Dinh, [a] Ta Ngoc Bach,[b] Nguyen Quang Hoa[c] and Anh-Tuan Le *[a]

Surface-Enhanced Raman Scattering (SERS) is a powerful analytical tool, which is usually based on the use of noble metal nanoparticles. To further improve the performance of SERS sensors, the substrates have been modified, leading to the design and development of metal–semiconductor nanocomposites. In this work, a series of zinc oxide–silver (ZnO/Ag) nanocomposites with different ZnO contents were prepared and employed for Raman measurements of ofloxacin (OFL) to evaluate their SERS performance. By comparing their SERS sensing performance, the effects of ZnO and ZnO content were clarified. With the most optimal ZnO content of 16 wt%, the ZnO/Ag-based SERS sensor could detect OFL at concentrations ranging from 10^{-3} M to 10^{-11} M in standard solutions, achieving an ultralow limit of detection (LOD) of 1.5×10^{-11} M. The SERS signal of OFL on ZnO/Ag substrate has been improved with the EF calculated to be 1.8×10^{6}, which is about 10 times higher than on pure AgNPs (1.7×10^{5}). This impressive enhancement was achieved by the effects of Ag (electromagnetic and chemical enhancement) and ZnO (adsorption), individually, as well as the combining effects of the two components (additional electromagnetic enhancement and charge transfer). Furthermore, the advanced SERS sensor based on ZnO/Ag nanocomposite substrate could determine OFL content in beef and a commercial OFL ophthalmic solution.

Received 2nd February 2025
Accepted 17th March 2025

DOI: 10.1039/d5ra00776c

rsc.li/rsc-advances

1. Introduction

Surface-Enhanced Raman Scattering (SERS) is a sensitive analytical tool that features molecular structural fingerprints and remarkably magnified Raman signals. The inelastic light scattering of molecules can be dramatically enhanced when they are adsorbed onto SERS substrates. An effective SERS substrate should provide active surfaces for both light–matter interaction and molecular adherence.[1] Thus, the design and development of the SERS substrate offers an effective solution to improve the efficiency of the Raman signal in identifying molecules.[2] The SERS enhancement is mainly attributed to two mechanisms: the electromagnetic mechanism (EM) and the chemical mechanism (CM).[3,4] The substrates are rich in free electrons which can create the excitation of localized surface plasmon resonance (LSPR), which is the main factor of EM and LSPR is related to the localized collective oscillation of electrons on the substrate. Therefore, with the highest free carrier densities, noble metals such as Ag, Au, and Cu are the most widely-used substrates for SERS study. Besides, the CM has also been proposed as a factor for SERS enhancement through the charge transfer (CT) process between substrate and probe molecule. The CT process in the substrate-to-molecule system is explained by the change in the electron density distribution of molecules leading to increasing polarizability and thus enhanced Raman scattering. Jensen *et al.* showed three types of CT contributions including the interfacial ground-state charge transfer (GSCT), the photoinduced charge transfer (PICT) resonance, and the electronic excitation resonance. The first, CT contribution is related to chemisorption interactions between the molecule and the substrate in the ground state absent of excitations, so it is a non-resonant contribution and called the

---

[a] *Phenikaa University Nano Institute (PHENA), Phenikaa University, Hanoi 12116, Vietnam. E-mail: anh.nguyenha@phenikaa-uni.edu.vn; tuan.leanh@phenikaa-uni.edu.vn*

[b] *Institute of Materials Science (IMS), Vietnam Academy of Science and Technology, 18 Hoang Quoc Viet, Hanoi 10000, Vietnam*

[c] *Center for Materials Science, Faculty of Physics, Ha Noi University of Science, Nguyen Trai Street, Hanoi 10000, Vietnam*

† Electronic supplementary information (ESI) available. See DOI: https://doi.org/10.1039/d5ra00776c

‡ D. T. N. Nga and H. A Nguyen contributed equally to this work.

GSCT pathway. The second, photo-induced charge transfer (PICT) concerns the energy-level matching between the metal (Fermi level) and probe molecule (the highest occupied/lowest unoccupied molecular orbital – HUMO/LUMO). The CT in this pathway is the transfer of hot electrons in the direction of metal to molecule or molecule to metal *via* photon excitations. Third, Resonance Raman Scattering (RRS) can occur when the laser excitation frequency is close to its electronic transition frequency.[5,6] Nowadays, many researchers pay special attention to the CT contribution to SERS enhancement by developing an active substrate to detect various analytes, such as functional metal–semiconductor nanocomposites.

There is a large amount of nanocomposites with noble metal–semiconductor constructions based on various semiconductors, such as TiO_2,[7] CuO,[8] Cu_2O,[9] MnO_2,[10] and ZnO.[11] In general, most of the proposed mechanisms of SERS enhancement based on metal–semiconductor substrates are both EM and/or CM,[12] among which the EM is related to the LSPRs in the noble metal nanostructures, and CM mainly originates from the CT in the semiconductor nanostructures.[13] The maximum enhancement factor (EF) for the EM contribution could reach 10^{11}, while this value for the CM contribution could only achieve 10^{4}.[14,15]

To fabricate nanocomposite substrates for SERS sensors, ZnO has been regarded a promising candidate to corporate with silver nanoparticles (AgNPs) in several recent reports.[16–18] In a study, Zeng *et al.* designed and developed a nanocomposite consisted of ZnO nanotower arrays and cubic and tetrahedral-shaped AgNPs to develop a SERS sensor detecting rhodamine 6G, exhibiting enormous SERS enhancement thanks to the formation of hot spots as well as the promotion of electron transfer.[19] Lai *et al.* designed and developed a heterostructure of AgNPs decorated on ZnO nanowire resulting in better SERS sensing performance to detect *p*-aminothiophenol, compared to the use of pure AgNPs. This nanostructure would generate more hot spots between neighboring AgNPs and ZnO nanowires, which help strongly improve the Raman signal.[20] In another study, Tran *et al.* prepared SERS substrates based on the decoration of AgNPs on ZnO nanoplates to sense methyl red at concentrations down to 5×10^{-8} M. The author claimed that the SERS mechanism based on the ZnO/Ag substrate has a large electromagnetic contribution compared to the Ag original substrate in which charge transfer plays a pivotal role.[12] These reports proposed mechanisms of SERS improvement in the presence of ZnO in the nanocomposite, in comparison to the use of pure AgNPs. However, ZnO contents and their effects were not discussed. Moreover, there were few experimental models to clarify the effects of ZnO.

Ofloxacin (OFL) is one of the most powerful members of the second generation of quinolone synthetic antibiotics for the treatment of various bacterial infections. Because of its excellent effectiveness, this antibiotic has been overused in animal husbandry. It has been reported to be a cause of the selection and transmission of resistant bacteria as well as antibiotic-resistance in farming community.[21] Furthermore, the accumulation of antibiotic residues in meat, milk, and eggs also puts consumers at the risk of as antibiotic-resistance. While OFL is still widely used in many different medications for human, include treating multidrug resistant tuberculosis, overusing and misusing it in farming is unacceptable. Therefore, it has been completely banned for veterinary use in China, ensuring its absence in animal-derived foods.

In this work, ZnO/Ag nanostructures at different ZnO contents were prepared by decorating AgNPs onto the surface of ZnO nanoparticles using an ultrasonic process. The results showed significant improvements in SERS intensity of OFL on ZnO/Ag, in comparison to pure Ag. The effects of ZnO and its contents on SERS performance of ZnO/Ag were also discussed. The enhancing mechanism was then proposed and clarified through some electrochemical measurements. In addition, the different ZnO contents in nanocomposite were optimized. With the most optimal ZnO content of 16 wt%, ZnO/Ag could detect OFL at concentrations ranging from 10^{-3} M to 10^{-11} M in standard solutions, achieving limit of detection (LOD) of 1.5×10^{-11} M. Furthermore, the SERS sensor based on ZnO/Ag substrate could determine OFL content in beef and a commercial OFL ophthalmic solution with high reliability, indicating its potentials for application in food safety and medication quality monitoring, respectively.

2. Materials and methods

2.1. Materials and SERS substrates

Sodium citrate dihydrate ($Na_3C_6H_5O_7 \cdot 2H_2O \geq 99.0$ wt%) was purchased from Xilong Scientific Co., Ltd, China. AgNPs were synthesized by our group's previous research.[22] OFL was provided by Sigma-Aldrich. All chemicals were used directly without further purification. All the experimental work was performed using double distilled water.

Aluminum (Al) substrate was prepared with dimensions of 1 cm × 1 cm × 0.2 cm with a surface-active area of diameter 0.2 cm. First, the substrates were immersed in 1 M dilute hydrochloric acid solution to remove oxide/hydroxide on the surface, and then washed with ethanol and double distilled water about 5 times by ultrasound for 15 minutes per time. Finally, the substrates were dried at room temperature.

2.2. Preparation of ZnO nanoparticles and ZnO/AgNPs

Two zinc cathodes were immersed and installed parallel in 200 mL of 0.2 M sodium citrate $Na_3C_6H_5O_7$ electrolyte solution. The anode and cathode electrodes were connected to a power supply (at 9-voltage) with an electrochemical time of 4 hours. A white solution is the product of the electrochemical process, which is a zinc oxide aqueous solution (ZnO). ZnO solution is stored at room temperature and utilized for the next experiments.

ZnO/Ag nanocomposites were synthesized using a simple ultrasonic method. Typically, ZnO solution (1 mg mL^{-1}) was poured into AgNP solution (1 mg mL^{-1}). These nanocomposites containing different amounts of AgNPs and ZnO were ultrasonicated for 20 minutes. AgNPs were prepared *via* a facile electrochemical method as displayed in our previous study.[22] Two silver plates were immersed vertically and face to face in a beaker containing 200 mL of a 0.1% $Na_3C_6H_5O_7$ solution.

Electrolysis was carried out at room temperature and the solution was mixed by magnetic stirring at 200 rpm for 2 hours. As a result, a dark-yellow colloidal Ag solution was obtained. ZnO/Ag nanocomposites with different contents marked as ZnO/Ag ZnO/Ag 8–92, ZnO/Ag 16–84, ZnO/Ag 33–67, ZnO/Ag 50–50, ZnO/Ag 67–33, ZnO/Ag 84–16, which contained 8%, 16%, 33%, 50%, 67%, and 84% of ZnO, respectively.

2.3. Characterization and SERS measurement

The morphology of synthesized samples was observed using scanning electron microscopy (SEM). The UV-vis spectrophotometer (HP 8453) was used to record the UV-vis optical absorption spectra in the wavelength range of 200–700 nm. The phase and chemical composition of the samples were investigated by Power X-ray Diffraction (XRD, Bruker D5005 X-ray diffractometer) with strictly monochromatized Cu Kα ($\lambda = 1.5406$ Å) at a voltage of 40 kV and a current of 30 mA. The composition and chemical properties of the samples were identified using Raman spectroscopy (Horiba Macro-RAM™) with 785 nm laser excitation.

OFL solutions were prepared in double distilled, achieving concentrations ranging from 10^{-3} M to 10^{-11} M. They could be preserved at 2 to 4 °C in 4 weeks. For each SERS measurement, 5 μL of OFL solution of a specific concentration was dropped directly onto the prepared Al substrates and dried naturally at room temperature. The SERS spectrum was the recorded using a Macro-RAM™ Raman spectrometer (Horiba). Raman measurements were acquired by means of a 100× objective with a numerical aperture of 0.90. The laser power was set to 45 mW at a 45° contact angle, with a focal length of 115 nm. An exposure time of 15 seconds was used with three accumulations. The experiment was repeated three times with every point of the SERS substrates.

Beef samples were purchased from a local market and then homogenized thoroughly by mincing and mashing before extraction. Subsequently, 5 g of the obtained beef sample was mixed with 10 mL of the double-distilled water using a vortex mixer and then ultrasonicated for 1 hour. The collected liquid was filtered by Whatman 11 μM filter paper. Finally, the known different amounts of OFL were added to the obtained liquid.

The OFL ophthalmic solution sample (OFL) was purchased from a local pharmacy containing the active ingredient of OFL 0.3% (3 mg mL^{-1}) as well as disodium hydrogen phosphate, water for injection, and acid citric to adjust pH.

2.4. Electrochemical measurements

All electrochemical measurements were conducted using an electrochemical workstation (Palmsens 4, PS Trace, Palmsens, The Netherlands) at room temperature (25 °C ± 2 °C). In order to evaluate the electrochemical properties of modified electrodes, cyclic voltammetry (CV) was performed in 0.1 M KCl containing 5 mM $[\mathrm{Fe(CN)_6}]^{3-/4-}$ at a scan rate of 50 mV s^{-1} with a potential range from −0.3 V to −0.6 V, and electrochemical impedance spectroscopy (EIS) was used in the frequency range of 0.01–50 kHz with 10 mV amplitude of the AC voltage in the 0.1 M KCl supporting electrolyte, containing 5 mM $[\mathrm{Fe(CN)_6}]^{3-/4-}$. The electrochemical behavior of OFL on the modified SPEs was evaluated by using CV measurements in an aqueous phosphate buffer electrolyte solution (PBS, 0.1 M) at a scan rate of 50 mV s^{-1} in the potential range from −1.1 to 0 V, $t_{\mathrm{equilibrium}} = 15$ s.

3. Results and discussion

3.1. Structure characterization of ZnO nanostructures and ZnO–Ag nanocomposite materials

The morphologies and size of ZnO nanosheets and ZnO/Ag nanocomposite were first investigated using SEM images, as shown in Fig. 1d and e. Fig. 1d displays a high density of the

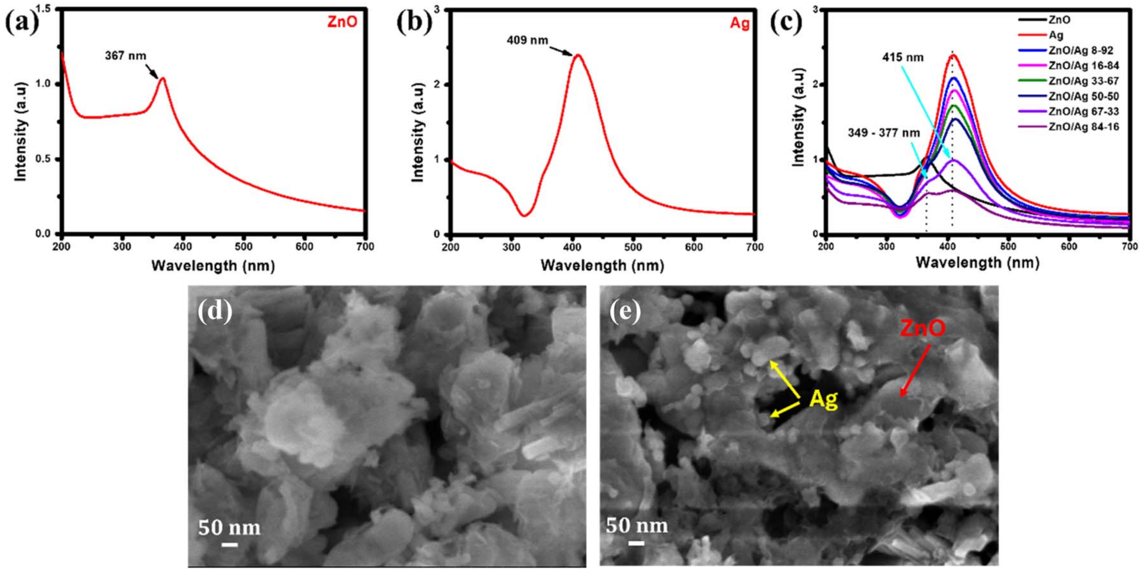

Fig. 1 UV-vis spectra of (a) ZnO nanosheets, (b) Ag NPs, and (c) pure Ag NPs, pure ZnO nanosheets, and ZnO/Ag nanocomposites with different ratios; SEM images of (d) ZnO nanosheets and (e) ZnO/Ag nanocomposite.

multi-layer stacked ZnO nanosheets with a width of around 300–500 nm and an average thickness of about 20–30 nm (Fig. S1†). Besides, the SEM image of ZnO/Ag nanocomposite is shown in Fig. 1e indicating that AgNPs with a diameter of about 40 nm were randomly distributed on the surface of ZnO nanosheets. The AgNPs were prepared in our previous study using the electrochemical method as described in Section 2.2.[22] ZnO nanosheets with a large surface area and plenty of wrinkles on their surface seem like a great platform for the anchoring of AgNPs.

Concerning other optical properties of the nanostructures, the absorption spectra of AgNPs, ZnO nanosheets, and ZnO/Ag nanocomposite were recorded. Fig. 1a shows absorption spectrum of ZnO nanosheets with a sharp peak at 367 nm. Meanwhile, the formation of AgNPs was confirmed by the presence of the characteristic peak at 409 nm in Fig. 1b. Fig. 1c compares absorption spectra of pure AgNPs, pure ZnO nanosheets and ZnO/Ag nanocomposites at different ratios. Different from pure AgNPs, ZnO/Ag nanocomposites exhibit a band at 415 nm. This red-shift could be a result of the electromagnetic coupling between the Ag and ZnO occurring the in-phase interactions between adjacent colloidal nanoparticles, lead to increasing charge magnitude of Ag and ZnO and possible different interactions with the synthesis medium.[23,24] In addition to the characteristic of AgNPs, ZnO/Ag nanocomposites also show a shoulder at around 349–377 nm, corresponding to the presence of ZnO nanosheets. With low Ag contents (*i.e.*, 16% and 33%), the shoulder is clearly observed. With higher Ag contents, the characteristic band of AgNPs is dominant.

For further investigation of the microstructures of synthesized samples, the deposition of AgNPs on ZnO nanosheets, and XRD measurements were conducted for comparison. As presented in Fig. 2, all peaks in the patterns of ZnO at $2\theta = 30.1°, 33.91°, 36.60°, 56.56°, 60.0°, 65.1°, 69.1°$ were identified as the characteristics diffraction peaks of the ZnO (JCPDS card no. 36-1451) and AgNPs are relevant with the standard diffraction peaks at $2\theta = 38.1°, 44.30°, 64.40°$ (JCPDS card no. 04-0783). The result indicates that all the contributions to Ag and ZnO phases existed in the XRD pattern of ZnO/Ag. The XRD pattern of ZnO and ZnO/Ag does not show strange peaks, which confirms the high purity and crystallization of ZnO and ZnO/Ag nanocomposite. Therefore, the synthesis process of AgNPs on the ZnO nanosheets surface is favorable and these nanocomposites were utilized for developing the SERS sensor in the next sections.

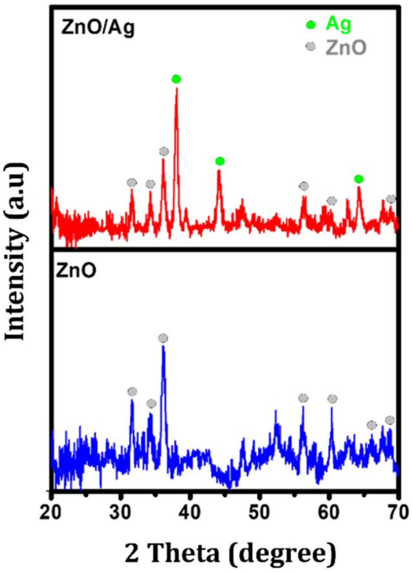

Fig. 2 XRD pattern of ZnO nanosheets (blue line), ZnO/Ag nanocomposite (red line).

3.2. Effects of the ZnO content on SERS performance

SERS spectra of OFL (10^{-5} M) on ZnO/Ag substrates with different ZnO contents are shown in Fig. 3a. It is necessary to identify the optimal ZnO content for optimizing the performance of these SERS sensors. Therefore, six types of ZnO/Ag nanocomposites were prepared containing 8, 16, 33, 50, 67 and 84 wt% of ZnO, named as ZnO/Ag 8–92, ZnO/Ag 16–84, ZnO/Ag 33–67, ZnO/Ag 50–50, ZnO/Ag 67–33, ZnO/Ag 84–16, respectively. The contents of ZnO and AgNPs were calculated based on the weight of each component added during preparation. The characteristic bands of OFL at 1407 cm^{-1} and 1626 cm^{-1} could be displayed in all the SERS spectra. The band at 1407 cm^{-1} is associated with the symmetric stretching mode of COO^-. The band at 1622 cm^{-1} was represented to the C–C tensile vibration of the aromatic quinoline ring.[24,25] Although the Raman spectrum of OFL powder had good correspondence with the SERS spectrum of OFL solution (Fig. S6†), some peak positions had minor changes. Especially, the absence of a characteristic peak at 1720 cm^{-1} in the SERS spectra of the OFL solution, while this absorption peak appeared with high intensity in the Raman spectra, which was mainly caused by the desiccation of the COOH group and the hydrogen bond formation between a carboxyl group and an adjacent ketone group. In addition, the most important characteristic peak for OFL Raman spectra of solid power was 1400 cm^{-1}, which had a minor shift in the OFL solution that it was in 1407 cm^{-1}. It was explained that the carboxyl was adsorbed on the silver substrate leading to the change of the symmetric stretching frequency of carboxyl.[26] Although characteristic peaks of OFL could be detected in all the SERS spectra, however, the SERS intensities of OFL on each substrate are clearly different. Fig. 3b shows the comparisons of SERS intensities at 1407 cm^{-1} and 1626 cm^{-1}. The results confirmed that the influence of ZnO on the performance of SERS sensors as with only 8 wt% of ZnO, SERS intensity of characteristic bands of OFL obviously increased. Moreover, this trend has maintained with the increase of the ZnO content in the nanocomposites to 16%. However, increasing the content of ZnO to 33 wt% and 50 wt% witnessed a significant decrease in SERS intensity, but the intensity was still higher than that on pure AgNPs. On nanocomposite substrates containing even higher ZnO contents of 67 wt% to 84 wt%, the SERS intensity of OFL decreases to levels lower than that on pure AgNPs (Fig. 3b). Because AgNPs is the key to SERS effect in this sensing platform, it is reasonable that on the nanocomposites containing high ZnO contents, and therefore, low Ag contents, SERS signal of OFL was reduced. Interestingly, the addition of ZnO nanosheets

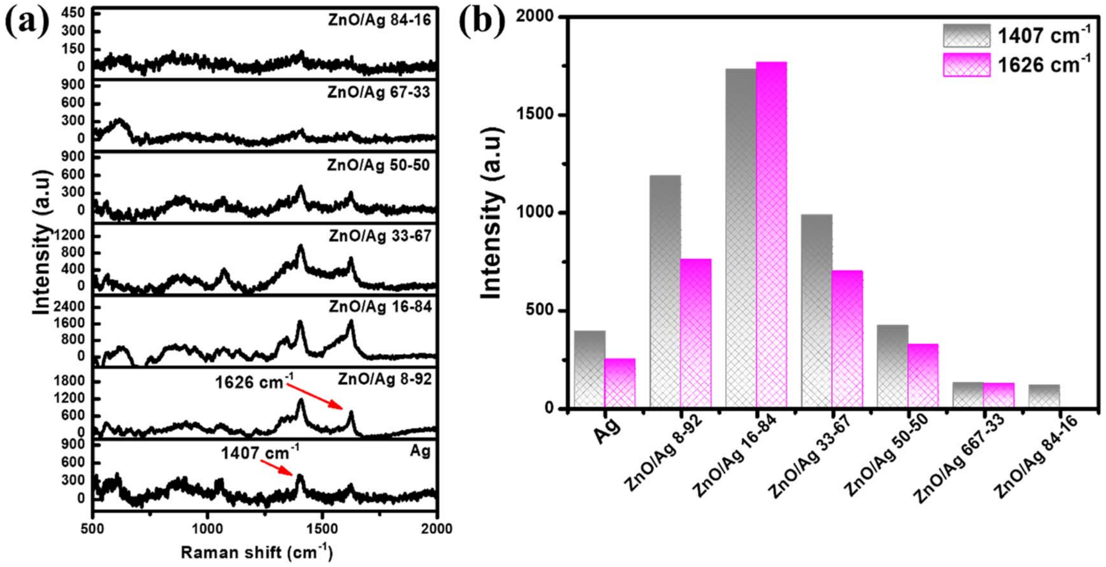

Fig. 3 (a) SERS spectra of OFL (10^{-5} M) on AgNPs, and ZnO/Ag nanocomposites with different ZnO contents. (b) SERS intensities of OFL (10^{-5} M) at 1407 and 1626 cm^{-1} on AgNPs, and ZnO/Ag nanocomposites with different ZnO contents.

at relatively low content led to significant improvement in SERS intensity of OFL. With the most impressive enhancement, ZnO/Ag 16–84 (16 wt% of ZnO) was chosen to further develop the high-performance SERS sensors.

3.3. The high-performance SERS sensors for OFL

The SERS spectra of OFL at nine concentrations (10^{-3} to 10^{-11} M) on ZnO/Ag 16–84 (16 wt% of ZnO) was shown in Fig. 4a. Characteristic bands of OFL could be detected in the spectra of OFL at concentrations as low as 10^{-10} M. When the concentration of OFL reaches 10^{-11} M, it is unable to detect any characteristic peaks of OFL. Fig. 4b displays a plot of logarithmic SERS intensity at 1407 cm^{-1} against the logarithmic concentration of OFL with a good linear relationship (linear regression of $R^2 = 0.98$) in the region from 10^{-10} M to 10^{-3} M. The LOD was calculated based on the linear equation to be 1.5

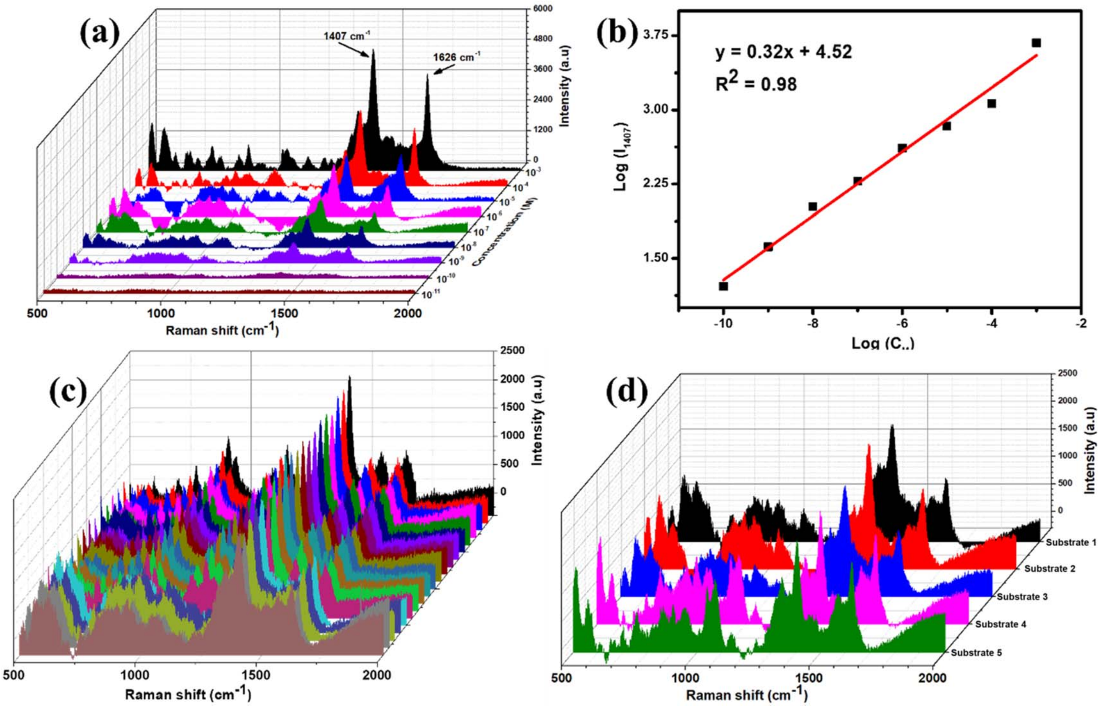

Fig. 4 (a) SERS spectra of OFL (10^{-3} to 10^{-11} M) on ZnO/Ag. (b) Plot of the log of SERS intensity at 1407 cm^{-1} against OFL concentration. (c) Uniformity and (d) reproducibility of SERS sensors for OFL (10^{-6} M) using the ZnO/Ag substrate (with 16 wt% of ZnO).

Table 1 Comparison of other OFL sensors

Nanostructure	LOD (M)	Linear range (M)	Ref.
Silver–molecularly imprinted polymers (AgNPs–MIPs)	10^{-10}	10^{-6} to 10^{-10}	29
AgNPs on thin-layer chromatography (TLC) plate	2.8×10^{-8}	—	20
Fe_3O_4@SiO_2@Ag–MIPs	10^{-8}	10^{-3} to 10^{-8}	27
TiO_2@Ag grafted thermo-sensitive imprinting material (TM@TiO_2@Ag)	1.1×10^{-11}	10^{-6} to 10^{-11}	30
Fe_3O_4–AuNCs–Cs@AgNPs	4.0×10^{-4}	—	28
Ag@PVA/Cs	10^{-5}	10^{-2} to 10^{-5}	31
ZnO/Ag nanocomposite	1.5×10^{-11}	10^{-6} to 10^{-10}	This work

$\times 10^{-11}$ M, which is lower than many reported noble Ag-based SERS sensors for OFL (Table 1). It confirms the effectiveness of this approach of material modification to prepare ZnO/Ag nanocomposites as advanced SERS active substrates. Besides, to investigate the stability of the ZnO/Ag substrate, a series of 10^{-6} M OFL SERS spectra were conducted from twenty different points on a substrate, as shown in Fig. 4c. There was no considerable difference in SERS intensity at 1407 cm^{-1}, indicating excellent stability of the SERS sensor system. The relative standard deviation (RSD) value was estimated to be 12.91%. In fact, the uniformity of this sensor is not as impressive as several reported ones such as Fe_3O_4@SiO_2@Ag–MIPs (3.53%)[27] and Fe_3O_4–AuNCs–Cs@AgNPs (<5.0%).[28] However, it is worth reminding that ZnO/Ag nanocomposites are the simplest to fabricate compared the others, which are required molecular imprinting technique or preparation of complex core–shell NPs. The RSD value of 12.91% is acceptable for uniformity of such a simply-prepared SERS sensor. Moreover, it is undeniable that ZnO/Ag nanocomposites allow the detection of OFL at lower concentrations (Table 1). In addition, the reproducibility of the method was confirmed by measuring the SERS signal of OFL (10^{-6} M) on five ZnO/Ag substrates using the same protocol, as shown in Fig. 4d. The RSD value was calculated to be 10.11% which shows the good reproducibility of the SERS sensor based on ZnO/Ag substrate.

3.4. Proposed roles of Ag and ZnO in the SERS signal enhancement of OFL using ZnO–Ag nanocomposites

SERS signal of OFL on ZnO/Ag were about 4–5 times higher in intensity than that on pure AgNPs. The differences in enhancement level of Raman signals induced by ZnO/Ag nanocomposites containing different ZnO contents confirmed that both ZnO nanosheets and AgNPs have played a significant role in improving SERS performance of the sensing system. However, while pure AgNPs could promote SERS effects, resulting in SERS signal of OFL, on ZnO/Ag composite with high ZnO content of 84 wt%, nearly all characteristic peaks of OFL have disappeared in the SERS spectrum. Therefore, Ag is still the key for SERS effect that occurred on ZnO/Ag substrates. However, the contribution of ZnO is undeniable.

Concerning the key to the effect, AgNPs, EM enhancements were induced around AgNPs. They are centers for enhanced electromagnetic fields, thanks to LSPR, which leads to a large improvement in the SERS performance of OFL. At the same time, CM enhancement would have been occurred *via* a PICT pathway between the substrate and the analyte in resonance with the excitation photons. This pathway can be relied on the relative locations of the Fermi level in AgNPs (−4.26 eV) and the highest occupied/lowest unoccupied molecular orbital (HOMO/LUMO – −4.88 eV/−4.08 eV) levels in the OFL molecule, which are calculated based on its onset oxidation and reduction potentials (ϕ_{ox} and ϕ_{red}) in phosphate buffered saline (PBS) solution (Fig. S2), respectively, as described in ESI.† Besides, the IGCT pathway made a minor contribution to the enhancements due to the formation of chemical bonding between AgNPs and the OFL molecule. El-Zahry and Lendl indicated that OFL molecules were chemisorbed on the silver surface through two sites: carboxylate group at C3 in quinoline ring and the non-binding electrons of the nitrogen N15 in piperazine ring (Fig. S3†).[26] This signal enhancement is a non-resonant contribution *via* the chemisorption interactions between the molecule and the substrate on the ground state in the absence of excitations. As a result, the combination of EM and CM enhancement, including both *via* PICT and IGCT pathway, has led to the enhancement factor of 1.7×10^5.

The semiconductor component of the nanocomposite also contributed to the overall SERS enhancement. To confirm that ZnO could be able to absorb the amount of OFL on the substrate surface, which helps improve the SERS sensor performance, we prepared an electrochemical model. Firstly, the adsorption capacity of the modified electrodes using pure AgNPs, ZnO/Ag 16–84 (16 wt% of ZnO), and ZnO/Ag 50–50 (50 wt% of ZnO) were investigated *via* cyclic voltammetric (CV) measurements in 0.1 M KCl containing 5 mM $[Fe(CN)_6]^{3-/4-}$ as a redox probe. As shown in Fig. S4,† a pair of redox peaks were displayed at all electrodes; however, the current intensity for each modified electrode was remarkably different, particularly, the highest current intensity observed at AgNPs_SPE, followed by ZnO/Ag 16–84_SPE, and ZnO/Ag 50–50_SPE. The further study on the change of CV response at three modified electrodes under varying scan rates from 0.01 to 0.05 V s^{-1}, it displayed the linear relationship between peak current (I – μA) and the square root of the scan rate ($\nu^{1/2}$ V s^{-1}), as shown in Fig. 5. Based on the corresponding slope of these line equations, the electroactive surface area (EASA) was calculated *via* the Randles–Sevcik formula:

$$I_p = (2.69 \times 10^5) n^{3/2} D^{1/2} A \nu^{1/2} C_0$$

where I_p is the peak current intensity, n is the number of electrons transfer ($n = 1$), D is the diffusion coefficient of

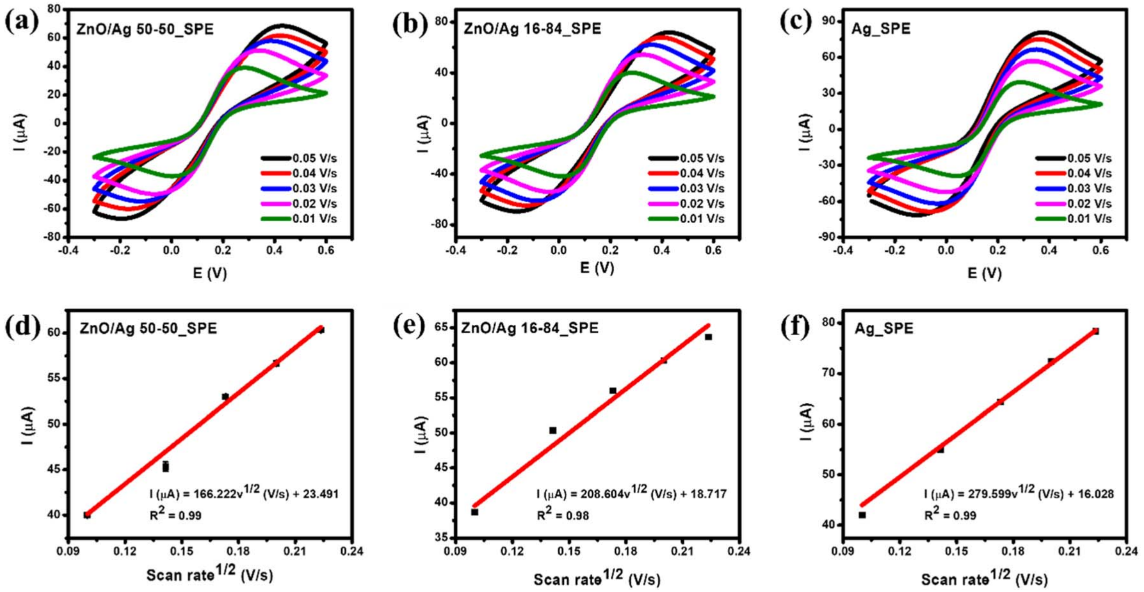

Fig. 5 CV curves recorded on ZnO/Ag 50–50_SPE (a), ZnO/Ag 16–84_SPE (b) and Ag_SPE (c) in 0.1 M KCl containing 5 mM $[Fe(CN)_6]^{3-}$/$[Fe(CN)_6]^{4-}$ with various scan rates from 0.01 to 0.05 V s^{-1}, corresponding calibration plots of peak current response *vs.* square root of scan rate (d–f) with error bars.

$[Fe(CN)_6]^{3-/4-}$ ($D = 6.5 \times 10^{-6}$ cm s^{-1}), A is the EASA value, n is the scan rate, and C refers to the bulk concentration of the redox probe. As a result, the AgNPs/SPE owned the highest EASA value of 0.082 cm^2 in comparison with the ZnO/Ag 16–84 (0.061 cm^2), and ZnO/Ag 50–50 (0.048 cm^2).

Subsequently, CV curves in 0.1 M PBS (pH = 7.2) containing 100 μM OFL analyte at the various scan rates in the range from 10 to 70 mV s^{-1} were carried out, as shown in Fig. 6. At all modified electrodes, the current response of the oxidation peak was significantly raised with an increase in the scan rate and a slight shift of peak potential. From these results, the corresponding regression equations were identified as follows:

$$I_p\ (\mu A) = 0.053\nu\ (\text{mV s}^{-1}) + 2.052\ (R^2 = 0.995) \text{ for Ag\_SPE}$$

$$I_p\ (\mu A) = 0.073\nu\ (\text{mV s}^{-1}) + 1.924\ (R^2 = 0.996) \text{ for ZnO/Ag 16–84\_SPE}$$

$$I_p\ (\mu A) = 0.081\nu\ (\text{mV s}^{-1}) + 2.309\ (R^2 = 0.991) \text{ for ZnO/Ag 50–50\_SPE}$$

From the linear relationships between I_p and ν, the adsorption capacity of OFL on the modified electrode surface with estimated EASE values was examined *via* the equation: $I_p = n^2F^2\nu A\Gamma/4RT$. Therefore, the Γ value calculated for each modified electrode from small to big was Ag_SPE (1.72×10^{-7} mol cm^{-2}) < ZnO/Ag 16–84_SPE (3.18×10^{-7} mol cm^{-2}) < ZnO/Ag 50–50_SPE (4.49×10^{-7} mol cm^{-2}). It is clear that the presence of ZnO in the nanocomposite enhanced a larger absorption capacity for OFL than the pure AgNPs, in which the Γ value of the ZnO/Ag 50–50_SPE was the highest and was 2.61-fold and 1.85-fold larger than the Ag_SPE, ZnO/Ag 16–84_SPE, respectively. The change in the electroactive surface area would be directly related to the change in the adsorption capacity of the targeted analyte. Consequently, the nanocomposites containing ZnO could absorb the largest number of OFL molecules compared to the pure AgNPs, which enhanced the chemical enhancement mechanism in SERS, leading to remarkably improved the SERS signal of OFL on ZnO/Ag substrate. However, ZnO/Ag 50–50 (50 wt% of ZnO) nanocomposite owns the best absorption capacity of OFL, but the SERS signal of OFL is slower than ZnO/Ag 16–84 (16 wt% of ZnO). This result reconfirmed the key role of Ag in the nanocomposite to generate SERS effect. Moreover, it clarified the role of ZnO in the nanostructure. By improving absorption capacity, on one hand, it allowed more OFL molecules to access and locate near AgNPs to experience SERS effects. Furthermore, with a carboxylic group in the molecular structure, OFL could have been chemisorbed onto ZnO nanosheets as described by Lubani *et al.*[32] In this 2022 study, the authors proposed adsorption models of carboxylic acids on ZnO *via* the formation of Zn–O bonds with two O atoms from the carboxylic groups. As a result, OFL could be attached onto ZnO nanosheets of ZnO/Ag composite *via* these chemical bonds, explaining the improvement in adsorption capacity thanks to the addition of ZnO into the nanocomposite.

Each component of the nanocomposite has exhibited excellent properties which could lead to the improvement of SERS sensing performance of the nanocomposite. Nevertheless, it was reported that their combination could eventually cause better enhancements. Lai *et al.* claimed that the additional EM enhancements were improved *via* the charge transfer between Ag and ZnO nanoparticles.[20] The Fermi level of Ag is −4.25 eV (ref. 33) and the conduction band of ZnO is −4.4 eV (ref. 34) compared to the vacuum level, as shown in Fig. S5.† The Fermi level of the metal always tends to achieve alignment *via* the heterostructure by electron transfer from the metal to the

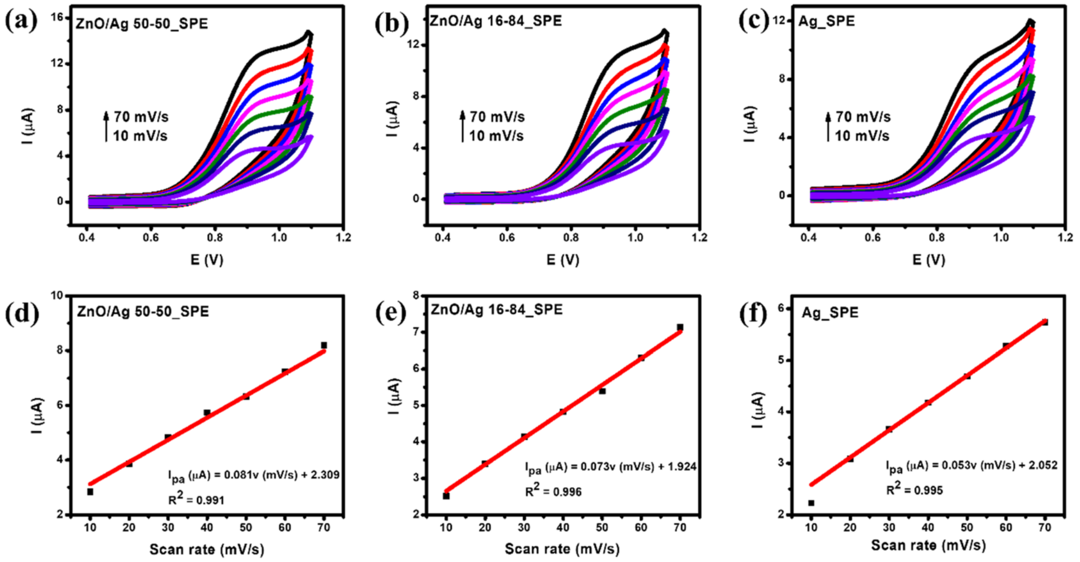

Fig. 6 (a–c) CVs responses of 100 μM ofloxacin at the modified electrodes in 0.1 M PBS buffer at different scan rates, and (d–f) plots of the peak current (*I*) *versus* scan rate (*v*).

semiconductor, which owns the conduction band lower than the Fermi level of the metal leading to the formation of a depletion region at the interface between the metal and the semiconductor. Herein, thanks to the motion of electrons flow from Ag to ZnO created a depletion zone, so the internal electric field is formed and leads to additional electromagnetic field enhancements for the SERS signal of OFL. Moreover, CM enhancements could also be improved thanks to the formation of Zn–O bonds, allowing more electrons to be transferred from Ag to OFL through the ZnO bridge. Accordingly, in the excitation of laser at 785 nm, electrons on the surface of AgNPs were excited and transferred to ZnO nanostructures *via* PICT pathway. Subsequently, these hot electrons could have continued to be transferred to OFL *via* IGCT pathway through Zn–O bonds as described in Fig. 7. This bond formation is in agreement with the disappearance of the band at 1720 cm^{-1} as mentioned in the previous section. Hence, SERS signal of OFL on ZnO/Ag has been improved with EF calculated to be 1.8×10^6, which is about 10 times higher than on pure AgNPs (1.7×10^5). ZnO/Ag nanocomposites, therefore, could be a suitable substrate for SERS detection of other carboxylic group-containing molecules.

3.5. Practicability of OFL based on ZnO–Ag

The practical feasibility of the SERS sensing system based on ZnO/Ag 16–84 was tested by determining certain concentrations of OFL in a complex food matrix (*i.e.*, beef). OFL solutions were spiked in beef samples to achieve five concentrations from 10^{-5} M and 10^{-9} M. Fig. 8a (left) shows the Raman spectra of the beef sample (red line) and the beef sample on the ZnO/Ag 16–84 substrate (black line). SERS spectra of OFL with five concentrations in beef samples on the ZnO/Ag 16–84 substrate were described in Fig. 8a (right). The intensities of the characteristic peak (1407 cm^{-1}) decreased for the real sample when the concentration of OFL in the real sample increased from 10^{-5} M to 10^{-9} M. Recovery rates range from 87% to 91% (Table S1†).

The practicability of the sensor was also evaluated by determining the concentration of OFL in a commercial eye drop

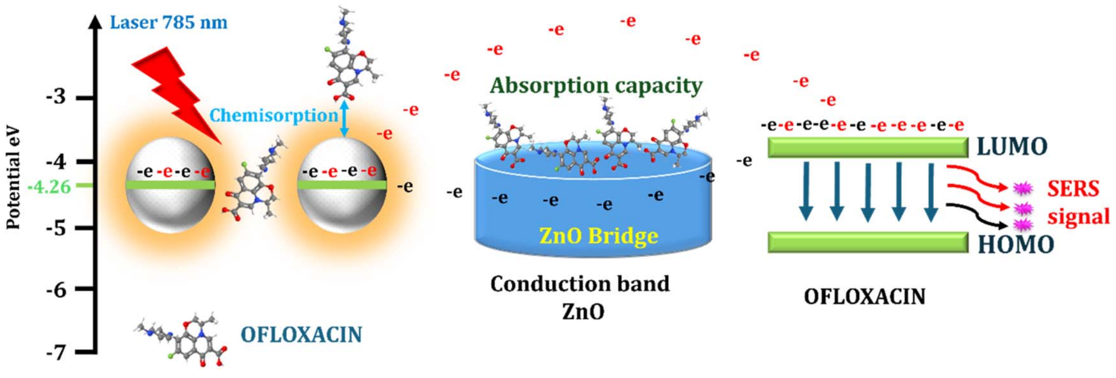

Fig. 7 Schematic proposed mechanism of charge transfer from ZnO/Ag to ofloxacin.

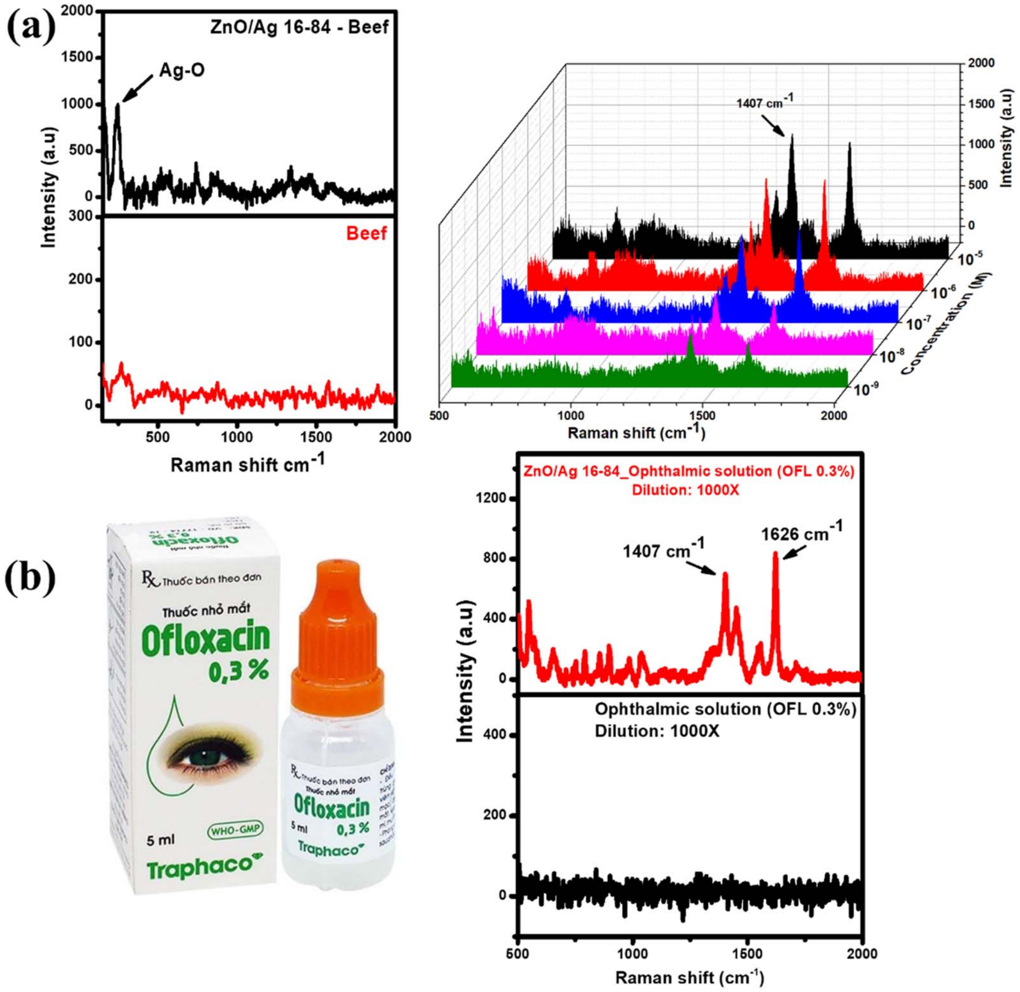

Fig. 8 (a) Raman spectra of beef sample (black line) on ZnO/Ag substrate in comparison to those of beef sample in the absence of ZnO/Ag (red line) (left); SERS spectra of OFL with different concentrations in real sample of beef on the ZnO/Ag SERS substrates (right); (b) 0.3 wt% OFL eye drop (left) and SERS spectra of 0.3 wt% OFL eye drop samples diluted 1000 times without and with the ZnO/Ag 16–84 SERS substrate (right).

available in Vietnam (Fig. 8b – left). The concentration of OFL in this ophthalmic solution was announced to be 0.3% (*i.e.*, 3 mg mL^{-1} to 8×10^{-3} M), which was not within the linear range from 10^{-3} M to 10^{-10} M. Therefore, the ophthalmic solution was diluted 1000 times. Fig. S7† shows Raman spectra of the original ophthalmic solution and several diluted ones. The two characteristic bands at 1407 cm^{-1} and 1626 cm^{-1} only appear in the Raman spectrum of the original ophthalmic solution with the highest concentration. As the ophthalmic solution was diluted to 10, 100 and 1000 times, those peaks disappear in their Raman spectra. Fig. 8b compares Raman spectrum of the 1000-time-diluted ophthalmic solution (black) and SERS spectrum of 1000-time-diluted ophthalmic solution on the ZnO/Ag substrate (red). While the Raman spectrum of the 1000-time-diluted ophthalmic solution exhibit no characteristic peak, the SERS spectrum of that solution on the ZnO/Ag substrate shows characteristic bands at 1407 cm^{-1} and 1626 cm^{-1}. In addition, the SERS spectrum also shows several new bands at 1034 cm^{-1}, 643 cm^{-1}, 784 cm^{-1}, 904 cm^{-1}, and 1468 cm^{-1}, which could be due to the presence of other compositions in the eye drops such as disodium hydrogen phosphate,[35] and acid citric.[36] The recovery value was calculated to be 90.01 ± 0.41%. These results indicated that ZnO/Ag can be employed as active substrate in SERS sensors to detect OFL in real samples for food safety and medication quality monitoring.

4. Conclusions

In this study, we fabricated ZnO/Ag nanocomposites with different Ag contents. The nanocomposites were employed as SERS substrates for OFL detection. On the substrates containing Ag contents equal to or higher than 50 wt%, SERS signal of OFL has been significantly improved, in comparison to that on pure AgNPs. This improvement could have been achieved thanks to the combination influence of both components. (i) AgNPs is the key for SERS effect of the nanocomposite which could induce SERS enhancement *via* both EM and CM (*i.e.*, PICT and IGCT pathways). (ii) ZnO nanosheets provide well-adsorbing platform for the chemisorption of OFL, which was confirmed by an electrochemical model. (iii) The combination of AgNPs and ZnO in nanocomposites promote SERS enhancements in both additional EM and CM enhancements. On one hand, the formation of a depletion region at the interface between the metal and the semiconductor leads to additional electromagnetic field enhancements for the SERS signal of OFL. Importantly, CM enhancements could also be improved thanks to the formation of Zn–O bonds, allowing more electrons to be transferred from Ag to OFL through the ZnO bridge. With the most optimal ZnO content of 16 wt%, ZnO/Ag could detect OFL at concentrations rage from 10^{-3} M to 10^{-11} M in standard solutions with an LOD of 1.5×10^{-11} M. Furthermore, the advanced SERS sensor based on ZnO/Ag substrate could determine OFL content in beef samples and a commercial OFL ophthalmic solution for food safety and medication quality monitoring, respectively.

Data availability

Data supporting this article have been included as part of the ESI.†

Author contributions

D. T. N. Nga: conceptualization, methodology, investigation, formal analysis, writing-original draft; H. A. Nguyen: conceptualization, methodology, investigation, formal analysis, writing-original draft; N. T. Hoa: validation, investigation, formal analysis; N. N. Huyen: validation, investigation, formal analysis; N. X. Dinh: validation, methodology, formal analysis; T. N. Bach: validation, investigation; N. Q. Hoa: validation, investigation; A. T. Le: conceptualization, methodology, supervision, project administration, writing-review & editing.

Conflicts of interest

The authors declare that they have no known competing financial interests or personal relationships that could have appeared to influence the work reported in this paper.

Acknowledgements

This research was acknowledged to the Phenikaa University through a fundamental research project PU2024-1-A-03. The authors would like to acknowledge the supports for Raman and Electrochemical measurements from NEB Lab (Phenikaa University), XRD from HUS-VNU and FE-SEM measurement from IMS-VAST.

References

1 S. Cong, X. Liu, Y. Jiang, W. Zhang and Z. Zhao, *Innovation*, 2020, **1**, 100051.

2 P. L. Stiles, J. A. Dieringer, N. C. Shah and R. P. Van Duyne, *Annu. Rev. Anal. Chem.*, 2008, **1**, 601–626.

3 N. L. Gruenke, M. F. Cardinal, M. O. McAnally, R. R. Frontiera, G. C. Schatz and R. P. Van Duyne, *Chem. Soc. Rev.*, 2016, **45**, 2263–2290.

4 K. A. Willets and R. P. Van Duyne, *Annu. Rev. Anal. Chem.*, 2007, **58**, 267–297.

5 L. Jensen, C. M. Aikens and G. C. Schatz, *Chem. Soc. Rev.*, 2008, **37**, 1061–1073.

6 J. R. Lombardi and R. L. Birke, *J. Phys. Chem. C*, 2014, **118**, 11120–11130.

7 J. S. Teguh, F. Liu, B. Xing and E. K. L. Yeow, *Chem.–Asian J.*, 2012, **7**, 975–981.

8 S. Hsieh, P.-Y. Lin and L.-Y. Chu, *J. Phys. Chem. C*, 2014, **118**, 12500–12505.

9 S. Sheng, Y. Ren, S. Yang, Q. Wang, P. Sheng, X. Zhang and Y. Liu, *ACS Omega*, 2020, **5**, 17703–17714.

10 D. T. Nguyet Nga, Q. D. Mai, N. Le Nhat Trang, M. K. Pham, N. Q. Hoa, V. D. Lam, H. Van Tuan, H. A. Nguyen and A.-T. Le, *Phys. Chem. Chem. Phys.*, 2023, **25**, 17496–17507.

11 Y. Wang, W. Ruan, J. Zhang, B. Yang, W. Xu, B. Zhao and J. R. Lombardi, *J. Raman Spectrosc.*, 2009, **40**, 1072–1077.

12 T. T. Tran, X. H. Vu, T. L. Ngo, T. T. H. Pham, D. D. Nguyen and V. D. Nguyen, *Phys. Chem. Chem. Phys.*, 2023, **25**, 15941–15952.

13 I. Alessandri and J. R. Lombardi, *Chem. Rev.*, 2016, **116**, 14921–14981.

14 H. Xu, J. Aizpurua, M. Käll and P. Apell, *Phys. Rev. E:Stat. Phys., Plasmas, Fluids, Relat. Interdiscip. Top.*, 2000, **62**, 4318–4324.

15 B. N. J. Persson, K. Zhao and Z. Zhang, *Phys. Rev. Lett.*, 2006, **96**, 207401.

16 H. Tang, G. Meng, Q. Huang, Z. Zhang, Z. Huang and C. Zhu, *Adv. Funct. Mater.*, 2012, **22**, 218–224.

17 J. Yin, Y. Zang, C. Yue, Z. Wu, S. Wu, J. Li and Z. Wu, *J. Mater. Chem.*, 2012, **22**, 7902–7909.

18 C. Liu, X. Xu, C. Wang, G. Qiu, W. Ye, Y. Li and D. Wang, *Sens. Actuators, B*, 2020, **307**, 127634.

19 Y. Zeng, F. Wang, D. Du, S. Liu, C. Wang, Z. Xu and H. Wang, *Appl. Surf. Sci.*, 2021, **544**, 148924.

20 Y.-C. Lai, H.-C. Ho, B.-W. Shih, F.-Y. Tsai and C.-H. Hsueh, *Appl. Surf. Sci.*, 2018, **439**, 852–858.

21 R. Si, Y. Yao, X. Liu, Q. Lu and M. Liu, *One Health*, 2022, **15**, 100448.

22 M. Q. Doan, N. H. Anh, N. X. Quang, N. X. Dinh, D. Q. Tri, T. Q. Huy and A.-T. Le, *J. Electron. Mater.*, 2022, **51**, 150–162.

23 C.-F. Chen, S.-D. Tzeng, H.-Y. Chen, K.-J. Lin and S. Gwo, *J. Am. Chem. Soc.*, 2008, **130**, 824–826.

24 L. M. Liz-Marzán, *Langmuir*, 2006, **22**, 32–41.

25 C. Ma and J. M. Harris, *Langmuir*, 2012, **28**, 2628–2636.

26 M. R. El-Zahry and B. Lendl, *Spectrochim. Acta, Part A*, 2018, **193**, 63–70.

27 Y. He, L. Li, X. Li and J. Zhang, *Chem. Lett.*, 2020, **49**, 713–716.

28 W. Hu, L. Xia, Y. Hu and G. Li, *Talanta*, 2024, **266**, 125057.

29 C. Jiang, T. Wu, J. Liu and Y. Wang, *Anal. Methods*, 2020, **12**, 4783–4788.

30 C. Jiang, T. Wu, X. He, Y. Wang and H.-z. Lian, *Chemosensors*, 2022, **10**, 437.

31 G. Huang, Y. Chen and Y. Li, *Dig. J. Nanomater. Biostruct.*, 2022, **17**, 171–178.

32 J. Lubani, F. De Angelis, D. Meggiolaro, L. Cartechini and S. Fantacci, *Molecules*, 2022, **27**, 3362.

33 M. Schnippering, M. Carrara, A. Foelske, R. Kötz and D. Fermín, *Phys. Chem. Chem. Phys.*, 2007, **9**, 725–730.

34 H. M. Abd El-Lateef, M. M. Khalaf, F. E. T. Heakal, M. F. Abou Taleb and M. Gouda, *Sol. Energy*, 2023, **253**, 453–461.

35 V. P. Padmanabhan, R. Kulandaivelu, D. Santhana Panneer, S. Vivekananthan, S. Sagadevan and J. Anita Lett, *Mater. Res. Innovations*, 2020, **24**, 171–178.

36 Z. Huang, X. Chen, Y. Li, J. Chen, J. Lin, J. Wang, J. Lei and R. Chen, *Appl. Spectrosc.*, 2013, **67**, 757–760.